

1 **Interhemispheric Effect of Global Geography on Earth's Climate Response to**  
2 **Orbital Forcing**

3 **Rajarshi Roychowdhury<sup>1</sup> and Robert DeConto<sup>1</sup>**

4 <sup>1</sup>University of Massachusetts - Amherst

5 *Correspondence to:* [rroychowdhur@geo.umass.edu](mailto:rroychowdhur@geo.umass.edu)

6 **Postal Address:**

7 Department of Geosciences

8 627 North Pleasant Street

9 233 Morrill Science Center

10 University of Massachusetts

11 Amherst, MA 01003-9297

12

13 **Abstract**

14 The climate response of the Earth to orbital forcing shows a distinct hemispheric asymmetry due  
15 to the unequal distribution of land in the Northern versus Southern Hemispheres. This  
16 asymmetry is examined using a Global Climate Model (GCM) for different climate responses  
17 such as Mean Summer Temperatures and Positive Degree Days. A Land Asymmetry Effect  
18 (LAE) is quantified for each hemisphere and the results show how changes in obliquity and  
19 precession translate into variations in the calculated LAE. We find that the global climate  
20 response to specific past orbits is likely unique and modified by complex climate-ocean-

21 cryosphere interactions that remain poorly known. Nonetheless, these results provide a baseline  
22 for interpreting contemporaneous proxy climate data spanning a broad range of latitudes, which  
23 maybe useful in paleoclimate data-model comparisons, and individual time-continuous records  
24 exhibiting orbital cyclicality.

## 25 **1. Introduction**

26 The arrangement of continents on the Earth's surface plays a fundamental role in the Earth's  
27 climate response to forcing. Due to the asymmetric global geography of the Earth, more  
28 continental land area is found in the Northern Hemisphere (68%) as compared to the Southern  
29 Hemisphere (32%). These different ratios of land vs. ocean in each hemisphere affect the balance  
30 of incoming and outgoing radiation, atmospheric circulation, ocean currents, and the availability  
31 of terrain suitable for growing glaciers and ice-sheets. Subsequently, the climate response of the  
32 Earth to radiative forcing is asymmetric (Figure 1b and 1c), while the radiative forcing (top-of-  
33 atmosphere solar radiation) itself is symmetric across the two hemispheres (Figure 1a). As a  
34 result of the inherent land-ocean asymmetry of the Earth, the climatic responses of the Northern  
35 and Southern Hemisphere differ for an identical change in radiative forcing (Barron et al., 1984;  
36 Deconto et al., 2008; Kang et al., 2014; Short et al., 1991).

37 Charles Lyell was the first to consider the influence of paleogeography on surface temperatures,  
38 in the context of the connection between climate and the modern distribution of land and sea  
39 (Lyell, 1832). By comparing the climates of the Northern and Southern Hemispheres and the  
40 distribution of land and sea, Lyell pointed out that the present continental distribution lowers  
41 high latitude temperatures in both hemispheres. He further pointed out that dominance of ocean  
42 in the Southern Hemisphere leads to mild winters and cool summers. Lyell's work is significant

43 in the context of this paper, because it first sparked the debate of continental forcing versus  
44 astronomical forcing of climate.

45 Since then, a number of classic studies have shown interhemispheric asymmetry in climate  
46 response of Northern and Southern Hemispheres. Climate simulations made with coupled  
47 atmosphere-ocean GCMs typically show a strong asymmetric response to greenhouse-gas  
48 loading, with Northern Hemisphere high latitudes experiencing increased warming compared to  
49 Southern Hemisphere high latitudes (Flato and Boer, 2001; Stouffer et al., 1989). GCMs also  
50 show that the Northern and Southern Hemispheres respond differently to changes in orbital  
51 forcing (e.g. Philander et al., 1996). While the magnitude of insolation changes through each  
52 orbital cycle is identical for both hemispheres, the difference in climatic response can be  
53 attributed to the fact that Northern Hemisphere is land-dominated while Southern Hemisphere is  
54 water dominated (Croll, 1870). This results in a stronger response to orbital forcing in the  
55 Northern Hemisphere relative to the Southern Hemisphere.

56 The distribution of continents and oceans have an important effect on the spatial heterogeneity of  
57 the Earth's energy balance, primarily via the differences in albedos and thermal properties of  
58 land versus ocean (Trenberth et al., 2009). The latitudinal distribution of land has a dominant  
59 effect on zonally averaged net radiation balance due to its influence on planetary albedo and  
60 ability to transfer energy to the atmosphere through long-wave radiation, and fluxes of sensible  
61 and latent heat. The latitudinal net radiation gradient controls the total poleward heat transport  
62 requirement, which is the ultimate driver of winds, and ocean circulation (Stone, 1978). Oceans  
63 have a relatively slower response to seasonal changes in insolation due to the higher specific heat  
64 of water as compared to land, and mixing in the upper ~10-150 m of the ocean. As a result, in the  
65 ocean-dominated Southern Hemisphere, the surface waters suppress extreme temperature swings

66 in the winter and provide the atmosphere with a source of moisture and diabatic heating. In the  
67 land-dominated Northern Hemisphere, the lower heat capacity of the land combined with  
68 relatively high albedo results in greater seasonality, particularly in the interiors of large  
69 continents of Asia and North America. The land surface available in a particular hemisphere  
70 also affects the potential for widespread glaciation, and the extreme cold winters associated with  
71 large continents covered by winter snow.

72 Continental geography has a strong impact on polar climates, as is evident from the very  
73 different climatic regimes of the Arctic and the Antarctic. Several early paleoclimate modeling  
74 studies using GCMs investigated continental distribution as a forcing factor of global climate  
75 (e.g. Barron et al., 1984; Hay et al., 1990). These studies demonstrated that an Earth with its  
76 continents concentrated in the low latitudes is warmer and has lower equator-to-pole temperature  
77 gradients than an Earth with only polar continents. Although these early model simulations did  
78 not incorporate all the complexities of the climate system, the results provided valuable insights  
79 from comparative studies of polar versus equatorial continents in the Earth and showed that  
80 changes in continental configuration has significant influence on climatic response to forcing.

81 The asymmetry in the climates of the Northern and Southern Hemispheres can be attributed to  
82 three primary causes: (i) Astronomical: Variation in insolation intensity across the Northern and  
83 Southern Hemispheres caused by the precession of the equinoxes (today perihelion coincides  
84 with January 3, just after the December 21 solstice, leading to slightly stronger summer  
85 insolation in the Southern Hemisphere); (ii) Continental geography: the effect of the continental  
86 geography on climate as described above; and (iii) Interhemispheric continental geography, i.e.  
87 the effect of Northern Hemisphere continental geography on Southern Hemisphere climate and  
88 vice-versa. The aim of this study is to gain a better understanding and isolate the effect of

89 interhemispheric continental geography on climate by comparing results from GCM simulations  
90 using modern versus idealized (hemispherically symmetric) global geographies. The GCM  
91 simulations with modern and idealized (symmetric) geographies are used to quantify the  
92 different climate responses to a range of orbits. By comparing the climatic response from  
93 simulations with different geographies, we isolate and estimate the effect of interhemispheric  
94 continental geography, i.e. the influence of one hemisphere's geography on the climate response  
95 of the opposite hemisphere.

96 One of the main caveats of this study is the lack of a dynamical ocean in our model setup. While  
97 this presents certain limitations, the model's computational efficiency has the advantage of  
98 allowing a wide range of orbital parameter space to be explored. We view the inclusion of a full  
99 depth dynamical ocean as a next step, hopefully motivated in part by the results published here.  
100 Furthermore, dynamical ocean models introduce an additional level of complexity and model-  
101 dependencies that we think are best avoided in this initial study.

## 102 **2. Model**

### 103 **2.1 Experimental design**

104 Global Climate Models (GCM) have been used extensively to study the importance of geography  
105 on the Earth's climate in the past. In this study, we use the latest (2012) version of the Global  
106 ENvironmental and Ecological Simulation of Interactive Systems (GENESIS) 3.0 GCM with a  
107 slab ocean component (Thompson and Pollard, 1997) rather than a full-depth dynamical ocean  
108 (Alder et al., 2011). The slab-ocean predicts sea surface temperatures and ocean heat transport as  
109 a function of the local temperature gradient and the zonal fraction of land versus sea at each  
110 latitude. While explicit changes in ocean currents and the deep ocean are not represented, the

111 computational efficiency of the slab-ocean version of the GCM allows numerous simulations  
112 with idealized global geographies and greatly simplifies interpretations of the sensitivity tests by  
113 precluding complications associated with ocean model dependencies. The ocean depth is limited  
114 to 50-m (enough to capture the seasonal cycle of the mixed layer). In addition to the atmosphere  
115 and slab-ocean, the GCM includes model components representing vegetation, soil, snow, and  
116 thermo-dynamic sea ice. The 3-D atmospheric component of the GCM uses an adapted version  
117 of the NCAR CCM3 solar and thermal infrared radiation code (Kiehl et al., 1998) and is coupled  
118 to the surface components by a land-surface-transfer scheme. In the setup used here, the model  
119 atmosphere has a spectral resolution of T31 ( $\sim 3.75^\circ$ ) with 18 vertical layers. Land-surface  
120 components are discretized on a higher resolution  $2^\circ \times 2^\circ$  grid.

121 The GCM uses various geographical boundary conditions (described below) in  $2^\circ \times 2^\circ$  and  
122 spectral T31 grids for surface and AGCM models, respectively. For each set of experiments, the  
123 model is run for 50 years. Spin-up is taken into account, and equilibrium is effectively reached  
124 after about 20 years of integration. The results used to calculate interhemispheric effects are  
125 averaged over the last 20 years of each simulation. Greenhouse gas mixing ratios are identical in  
126 all experiments and set at preindustrial levels with  $\text{CO}_2$  set at 280 ppmv,  $\text{N}_2\text{O}$  at 288 ppbv and  
127  $\text{CH}_4$  at 800 ppbv (Meinshausen et al., 2011). The default values for  $\text{CFCl}_3$  and  $\text{CF}_2\text{Cl}_2$  values are  
128 set at 0 ppm. The solar constant is maintained at  $1367 \text{ Wm}^{-2}$ .

## 129 **2.2 Asymmetric and symmetric Earth geographies**

130 The GCM experiments are divided into three sets: 1) Preindustrial CONTROL 2) NORTH-  
131 SYMM and 3) SOUTH-SYMM. The Preindustrial CONTROL experiments use a modern global  
132 geography spatially interpolated to the model's  $2^\circ \times 2^\circ$  surface grid (Cuming and Hawkins, 1981;  
133 Kineman, 1985). The geographical inputs provide the land-ice sheet-ocean mask and land–

134 surface elevations used by the GCM, along with global maps of vegetation distribution, soil  
135 texture and other quantities (Koenig et al., 2012).

136 To simulate the climate of an Earth with meridionally symmetric geographies, we created two  
137 sets of land surface boundary conditions: NORTH-SYMM and SOUTH-SYMM. For the  
138 NORTH-SYMM experiments, the CONTROL experiment boundary conditions are used to  
139 generate a modified GCM surface mask, by reflecting the Northern Hemisphere geography  
140 (land-sea-ice mask, topography, vegetation, soil texture) across the equator into the Southern  
141 Hemisphere. Similarly, in the experiment SOUTH-SYMM, the land mask and geographic  
142 boundary conditions in the Southern Hemisphere are mirrored in the Northern Hemisphere. The  
143 NORTH-SYMM and SOUTH-SYMM boundary conditions are shown in Figure 2b and 2c, with  
144 the CONTROL (Figure 2a) for comparison. Poleward oceanic heat flux is defined as a function  
145 of the temperature gradient and the zonal fraction of land and sea at given latitude in the model;  
146 hence the parameterized ocean heat flux is symmetric in our symmetrical Earth simulations.

### 147 **3. Symmetry (and asymmetry in GCM results)**

148 In the first experimental setup, we run the GCM with modern day orbital configuration, i.e.  
149 eccentricity is set at 0.0167, obliquity is set at 23.5° and precession such that perihelion  
150 coincides with Southern Hemisphere summer. The radiation at Top-of-Atmosphere is shown in  
151 terms of mean summer insolation and Summer Energy (Figure 3a and 3b). The Summer Energy is  
152 an integrated measure of changes in insolation intensity as well as duration of summer, and is defined as  
153  $J = \sum_i \beta_i (W_i \times 86,400)$ , where  $W_i$  is mean insolation measured in  $W/m^2$  on day  $i$ , and  $\beta$  equals one when  
154  $W_i \geq \tau$  and zero otherwise.  $\tau = 275 W/m^2$  is taken as the threshold for melting to start at the surface of the  
155 earth. Mean Summer Temperature (ST) is calculated from the GCM as the mean of the average  
156 daily temperatures for the summer months in each hemisphere. We define summer by an

157 insolation threshold ( $325 \text{ W/m}^2$ ); which accounts for the astronomical positions as well as the  
158 phasing of the seasonal cycle of insolation. The zonal averages of ST (calculated at each latitude)  
159 demonstrate the inherent asymmetry in the Earth's climate between Northern and Southern  
160 Hemispheres, especially evident in the higher latitudes (Figure 3c). Positive Degree Days (PDD)  
161 captures the intensity as well as the duration of the melt season, and has been shown to be  
162 indicative of ice-sheet response to changes in external forcing. Figure 3d shows the PDD for  
163 modern orbit, with zonal averages plotted in the log scale. The asymmetry between the Northern  
164 and Southern Hemispheres is captured by the GCM in the calculated PDDs.

165 Next, we maintain the modern orbit to test the effect of meridionally symmetric continents  
166 (Figure 3e-h). Figure 3e and 3f show ST and PDD from a simulation in which the Northern  
167 Hemisphere geography is reflected in the Southern Hemisphere (thus making the Earth  
168 geographically symmetric). Figure 3g and Figure 3h show ST and PDD from the simulation with  
169 symmetric Southern Hemisphere continents. Symmetric continents make the climates of  
170 Northern and Southern Hemispheres symmetric (>95%). However, due to the current timing of  
171 perihelion with respect to the summer solstices, there remains some minor asymmetry. Using an  
172 orbit in which perihelion coincides with equinoxes will make the climate truly symmetrical.

## 173 **4. Modern Orbit Simulations**

### 174 **4.1 Effect of Southern Hemisphere (SH) on Northern Hemisphere (NH) climate**

175 To estimate the effect of SH continental geography on NH climate, we subtract the NH climate  
176 of the NORTH-SYMM simulation (symmetric Northern continents in both hemispheres) from  
177 the CONTROL simulation (asymmetric, modern orbit). In these two simulations, the only  
178 difference in setup is the Southern Hemispheric continental distribution. Thus the difference in



179 NH climate from the two simulations, if any, can be safely ascribed as the effect of SH  
180 continental geography on NH climate. We quantify this interhemispheric effect for ST (for NH)  
181 as:

$$182 \quad e_{\widehat{Summer Temp}} = \frac{1}{n} \sum_i^n (T_i^{control} - T_i^{north}) \quad \dots(1)$$

183 Analogous to the effect for ST, the effect for PDD, which we call the “Land Asymmetry Effect”  
184 (LAE), is defined as follows:

$$185 \quad LAE_{(NH)} = PDD^{control} - PDD^{north} \quad \dots(2)$$

186 Where  $T_i^{control}$  and  $PDD^{control}$  are the mean daily temperature and PDD from the CONTROL  
187 simulation, and  $T_i^{North}$  and  $PDD^{North}$  are the mean daily temperature and PDD from the simulation  
188 with the North-symmetric geography (NORTH-SYMM). ‘n’ is the number of days in the  
189 summer months in each hemisphere.

#### 190 **4.2 Effect of Northern Hemisphere (NH) on Southern Hemisphere (SH) climate**

191 Similarly, we estimate the effect of NH continental geography on the SH by subtracting the SH  
192 climate of the SOUTH-SYMM simulation (symmetric southern continents in both hemispheres)  
193 from the CONTROL simulation (asymmetric, modern orbit). In these two simulations, the  
194 differences in SH climate in the CONTROL and SOUTH-SYMM simulations, if any, can be  
195 ascribed as the ‘effect of NH continental geography on SH climate’. We quantify this  
196 interhemispheric effect for ST (for SH) and the LAE as:

$$197 \quad e_{\widehat{Summer Temp}} = \frac{1}{n} \sum_i^n (T_i^{control} - T_i^{south}) \quad \dots(3)$$

198  $LAE_{SH} = PDD^{control} - PDD^{south}$  ... (4)

199 where  $T_i^{control}$  and  $PDD^{control}$  are the mean daily temperature and PDD from the CONTROL  
200 simulation, and  $T_i^{south}$  and  $PDD^{south}$  are the mean daily temperature and PDD from the simulation  
201 with the south-symmetric geography (SOUTH-SYMM).

### 202 4.3 Results of Modern Orbit Simulations

203 Figure 4a and 4b show the interhemispheric effect of continental geography on ST and PDD  
204 respectively. For the Northern Hemisphere, the summer temperatures are calculated when the  
205 insolation intensity over the Northern Hemisphere is strongest. The asymmetry in the Southern  
206 Hemisphere landmasses leads to weakening of the summer warming over North America and  
207 Eurasia (blue shaded regions correspond to cooling). Consequently, summer temperatures over  
208 Northern Hemisphere continents are lower by 3-6°C relative to a symmetric Earth. There is a  
209 positive warming effect in the North-Atlantic Ocean, and in general the Northern Hemisphere  
210 oceans are slightly warmer relative to a symmetric Earth. The general trends in the  
211 interhemispheric effect on PDD (LAE) (Figure 4b) mimic those of the summer temperatures  
212 (Figure 4a).

213 For the Southern Hemisphere, the summer temperatures are calculated when the insolation is  
214 most intense over the Southern Hemisphere during the year. Southern Hemisphere landmasses,  
215 except Antarctica, generally show a cooling response during summer, due to Northern  
216 Hemisphere geography. Over Antarctica, summer temperatures are higher in the control  
217 simulations than in the symmetric simulations, leading to the inference that there is a warming  
218 (increase) in summer temperatures due to interhemispheric effect. Also, the Southern Ocean  
219 shows a strong positive temperature effect (warming) relative to a symmetric Earth, although this

220 Southern Ocean response might be different or modified if a full-depth dynamical ocean model  
221 were used.

## 222 **5. Idealized Orbit Simulations**

223 Next, we examine the effect of the opposite hemisphere on the Earth's climate response at  
224 extreme obliquities (axial tilt) and idealized precessional configurations (positions of the  
225 solstices and equinoxes in relation to the eccentric orbit). The orbital parameters used in these  
226 experiments are idealized and do not correspond to a specific time in Earth's history. Rather,  
227 they are chosen to provide a useful framework for studying the Earth's climate response to  
228 precession and obliquity. HIGH and LOW orbits approximate the highest and lowest obliquity in  
229 the last three million years (Berger and Loutre, 1991). NHSP (Northern Hemisphere Summer at  
230 Perihelion) and SHSP (Southern Hemisphere Summer at Perihelion) orbits correspond to  
231 Northern and Southern summers coinciding with perihelion, respectively. The other two  
232 precessional configurations considered are EP1 and EP2, with the perihelion coinciding with the  
233 equinoxes. For the idealized precession simulations, the obliquity is set at its mean value  
234 averaged over the last 3 million years. Eccentricity is set at the same moderate value (mean  
235 eccentricity over the last 3 million years) for all simulations. Table 1 summarizes the orbits used  
236 in the ensemble of model simulations. Here, we focus only on the LAE, as PDD is a better  
237 indicator of air temperature's influence on annual ablation over ice-sheets than summer  
238 temperature, since this metric captures both the intensity and duration of the melt season.

239 Changes in precession primarily affect seasonal insolation intensity that is well known to be out-  
240 of-phase in both hemispheres (Lyell, 1832). To demonstrate an asymmetry in the climate  
241 response to precession, we take the differences between two arbitrarily chosen extremes in the  
242 precession cycle (NHSP and SHSP) for both the forcing and the climate response. The forcing

243 (summer energy (J)) calculated at the top of the atmosphere is numerically symmetric (but out-  
244 of-phase as expected) in both hemispheres (Figure 5a). The difference in the PDDs  
245 ( $\Delta\text{PDD}_{\text{precession}}$ ) is the Earth's climate response to the combined effect of the two precessional  
246 motions (wobbling of the axis of rotation and the slow turning of the orbital ellipse). The climate  
247 response ( $\Delta\text{PDD}_{\text{precession}}$ ) is asymmetric across both hemispheres (Figure 5b). However, when we  
248 run the precessional simulations in a Earth with symmetric continents, the climate response to  
249 precession is symmetrical (Figure 5c and 5d).

250 In contrast to precession, obliquity alters the seasonality of insolation equally in both  
251 hemispheres (Figure 5e). A reduction in the tilt from  $24.5^\circ$  (HIGH) to  $22^\circ$  (LOW) reduces  
252 annual insolation by  $\sim 17 \text{ W/m}^2$  and summer insolation by  $\sim 45 \text{ W/m}^2$  in the high latitudes. In the  
253 tropics, summer insolation increases by up to  $\sim 5 \text{ W/m}^2$ . Loutre et al. (2004) among others  
254 predicted that global ice volume changes at the obliquity periods could be interpreted as a  
255 response to mean annual insolation and meridional insolation gradients. To demonstrate  
256 asymmetry in the climate response to obliquity, we take the differences between the highest and  
257 lowest obliquities for both the forcing and the climate response. The difference in the PDDs  
258 ( $\Delta\text{PDD}_{\text{obliquity}}$ ) is the Earth's climate response to changes in tilt. Figure 5f shows  $\Delta\text{PDD}_{\text{obliquity}}$   
259 and the zonal averages reveal the asymmetry in the obliquity climate response. The same  
260 simulations with North-symmetric Earth (Figure 5g) and South-symmetric Earth (Figure 5h)  
261 produce symmetrical climate responses to the obliquity cycle.

## 262 **6. Results of Idealized Orbit Simulations**

263 The effect of SH continental geography on NH at the idealized orbits is estimated using the same  
264 method described above, with the LAE for a given orbit (for NH) calculated as:

265  $LAE_{(NH)} = PDD_{orbit}^{control} - PDD_{orbit}^{north}$  ... (5)

266 Similarly, the effect of NH continental geography on SH at the idealized orbits is estimated using  
267 the same method described above, with the LAE for a given orbit (for SH) calculated as:

268  $LAE_{(SH)} = PDD_{orbit}^{control} - PDD_{orbit}^{south}$  ... (6)

269 Figure 6a shows the spatial variation of LAE when perihelion coincides with Northern  
270 Hemisphere summer (NHSP). The Northern Hemisphere landmasses show a strong negative  
271 response. In this orbit, the Northern Hemisphere experiences elevated summer insolation, but the  
272 response is attenuated by the interhemispheric effect. This dampening effect is greatest in the  
273 interiors of the Northern Hemisphere continents. If precession is considered in isolation (i.e.  
274 constant obliquity), according to the astronomical theory of climate the Northern Hemisphere  
275 should experience ‘interglacial’ conditions when perihelion coincides with Northern summer.  
276 However, because of the interhemispheric effect, interglacial (warm summer) conditions are  
277 muted relative to those on a symmetric Earth. During this orbit, the Southern Hemisphere  
278 experiences ‘glacial’ (cold summer) conditions due to the weaker summer insolation. The  
279 positive effect in the Southern Hemisphere leads to weaker cooling relative to a symmetric Earth.  
280 Thus, when perihelion coincides with Northern Hemisphere summer, the interhemispheric effect  
281 dampens the magnitude of ‘glacial’ versus ‘interglacial’ conditions in both hemispheres.

282 Figure 6b shows the spatial variation of LAE when perihelion coincides with Southern  
283 Hemisphere summer (SHSP). The Northern Hemisphere continents have a weak positive effect,  
284 leading to slightly warmer conditions relative to a symmetric Earth. In this orbit, the southern  
285 high latitudes experience intense summer insolation. The positive warming effect amplifies the  
286 already warm conditions in the Southern Hemisphere. Figures 6c and 6d show the spatial

287 variation of LAE at the two equinoxes respectively, i.e. when Northern Hemisphere vernal  
288 equinox is at perihelion (EP1) and when Northern Hemisphere autumnal equinox is at perihelion  
289 (EP2). The LAE is in general weaker at the equinoxes than at the solstices.

290 At HIGH obliquity, there exists a negative effect on Northern Hemisphere continents (Figure  
291 6e), which mutes the strong insolation intensity during summer months. In the Northern  
292 Hemisphere, as a result of continental asymmetry, a decrease in the equator to pole temperature  
293 gradient is observed. A lowering of summer temperatures and temperature gradient due to the  
294 interhemispheric effect has a negative impact on the deglaciation trigger associated with HIGH  
295 obliquity orbits. Thus the interhemispheric effect would hinder the melting of ice during high-  
296 obliquity orbits. In the Southern Hemisphere, the positive interhemispheric effect on PDD over  
297 Antarctica and the Southern Ocean leads to overall higher temperatures in the high southern  
298 latitudes as compared to a symmetric Earth. Thus, during the high obliquity orbits, positive effect  
299 helps deglaciation.

300 At LOW obliquity, the negative effect over Northern Hemisphere continents is generally less  
301 intense (Figure 6f). However, even the modest lowering of summer temperatures caused by the  
302 interhemispheric effect would support the growth of ice sheets during low obliquity orbits. The  
303 positive effect (warming) in the high Southern latitudes would delay the growth of ice sheets.

## 304 **7. LAE for orbital cycles**

305 Next, we calculate the LAE for a transition through a precessional cycle. We take two arbitrary  
306 end points in the precessional cycle (NHSP and SHSP), and calculate the difference of PDDs  
307 between the two simulations ( $\Delta\text{PDD}_{\text{precession\_cycle}}$ ). The LAE for precessional cycle is therefore  
308 calculated as:

309  $LAE_{(NH)} = \Delta PDD_{precession\_cycle}^{control} - \Delta PDD_{precession\_cycle}^{north} \dots(7)$

310  $LAE_{(SH)} = \Delta PDD_{precession\_cycle}^{control} - \Delta PDD_{precession\_cycle}^{south} \dots(8)$

311 The LAE shows a strong negative effect in the Northern Hemisphere (Figure 7a). For the  
 312 Northern Hemisphere, this transition from SHSP to NHSP equates to a transition from cool to  
 313 warm climate. The negative interhemispheric effect decreases the  $\Delta PDD$  in the real Earth, thus  
 314 weakening the effect of precession in the Northern Hemisphere. The Southern Hemisphere  
 315 shows a positive effect on PDD at high latitudes. For the Southern Hemisphere, the transition  
 316 from SHSP to NHSP equates to a transition from warmer to cooler climate. The positive  
 317 interhemispheric effect at high latitudes decreases the  $|\Delta PDD|$  in the real Earth, thus weakening  
 318 the effect of precessional cycle in the Southern Hemisphere high latitudes.

319 To calculate the LAE for a transition through the obliquity cycle, we take the highest and lowest  
 320 obliquities (HIGH and LOW), and calculate the difference of PDDs between the two simulations  
 321 ( $\Delta PDD_{obliquity\_cycle}$ ). The LAE for obliquity cycle is therefore calculated as:

322  $LAE_{(NH)} = \Delta PDD_{obliquity\_cycle}^{control} - \Delta PDD_{obliquity\_cycle}^{north} \dots(9)$

323  $LAE_{(SH)} = \Delta PDD_{obliquity\_cycle}^{control} - \Delta PDD_{obliquity\_cycle}^{south} \dots(10)$

324 The Northern Hemisphere shows a small negative effect in the high latitudes, and a positive  
 325 effect in the low latitudes (Figure 7b). The transition from LOW to HIGH corresponds to a  
 326 transition from cold to warm climate. The negative interhemispheric effect decreases the  $\Delta PDD$ ,  
 327 thus weakening the climate response of obliquity cycle in the high latitudes. The positive  
 328 interhemispheric effect increases the  $\Delta PDD$ , thus strengthening the climate response of obliquity  
 329 cycle in the low latitudes in the Northern Hemisphere. The Southern Hemisphere shows largely a

330 negative effect, with a positive effect in the high latitudes. The transition from LOW to HIGH  
331 corresponds to a transition from cold to warm climate. The positive interhemispheric effect  
332 increases the  $\Delta$ PDD, thus amplifying the effect of obliquity over Antarctica.

### 333 **8. Impact of various climatological variables on LAE**

334 A comprehensive, mechanistic evaluation of the hemispheric effect is beyond the scope of this  
335 initial study. However, as a first step, we test the relationship between the hemispheric LAE and  
336 various atmospheric processes by exploring correlations between the inter hemispheric responses  
337 to orbital forcing, and climatological fields related to changes in radiation (clouds), dynamics  
338 (heat and moisture convergence), and feedbacks related to surface processes (sea ice and snow  
339 albedo).

340 Numerous studies have shown the impact of variation in distribution of clouds (e.g., Meleshko  
341 and Wetherald, 1981) on climate. It is observed that the cloud cover changes in idealized  
342 symmetric continent experiments, i.e. the hemispheric asymmetry in the continental geography  
343 impacts the distribution of cloud cover, measured as the mean of total cloudiness. Cloud cover  
344 affects the climate through two opposing influences; a cooling effect is produced due to  
345 reflection of solar radiation, and a warming effect on climate due to reduction of effective  
346 temperature for outgoing terrestrial (longwave) radiation (Wetherald et al., 1980). However, the  
347 overall effect of increasing cloud cover is generally considered to cause cooling (Manabe et al.,  
348 1967; Schneider, 1972). The hemispheric asymmetry impacts the cloud cover fraction by as  
349 much as 10% at various latitudes (Figure 8a). The effect of asymmetry increases cloudiness over  
350 land poleward of 50° N latitude, contributing to negative net radiation and temperature anomalies  
351 over the Northern Hemisphere continents, and can be observed both in terms of Summer  
352 Temperatures and the PDD. In the Southern Hemisphere, total cloudiness decreases over the



353 Southern Ocean due to hemispheric asymmetry, contributing to a positive temperature anomaly  
354 over this region. At latitudes below 50 degrees, the increase in the area-mean flux of outgoing  
355 terrestrial radiation is almost compensated by the increase in net insolation flux. Thus, we expect  
356 minor impact of cloud content on the LAE at lower latitudes.

357 Snow cover reflects ~80 to 90% of the sun's energy and it has an important influence on energy  
358 balance and regional water budgets. Snow cover's effect on surface energy balance has a strong  
359 cooling effect, and conversely, decreasing snow cover leads to a decrease of surface albedo and  
360 warming. We find that the snow fraction (annual and monthly averages) is also influenced by the  
361 hemispheric asymmetry of the continents. There is a decrease in the snow fraction over most of  
362 Eurasia and North America due to hemispheric asymmetry (Figure 8c), leading to warming in  
363 the asymmetrical Earth when compared to an Earth with symmetric continents. The effect is  
364 more pronounced in the spring months (Figure 8d), which leads to longer summers, increasing  
365 the Positive Degree Days (PDD) in the asymmetric Earth. The relationship between the snow  
366 fraction and temperature anomalies is expected to be weaker in the heavily forested regions (such  
367 as Northern Asia), where the snow-albedo feedback is less effective (Bonan et al., 1992).  
368 Similarly, fractional sea ice cover has an opposing effect on temperature. Thus, an increase in  
369 fractional sea ice cover due to hemispheric asymmetry causes a negative LAE, as increased  
370 albedo reduces net shortwave radiative flux.

371 Spatial patterns in the LAE are compared with basic dynamical effects of the different  
372 geographies. Sea level pressure shows an effect due to hemispheric asymmetry (Figure 8g), with  
373 a general increase in the Northern Hemisphere and a decrease in the Southern Hemisphere. The  
374 resulting change in the time-averaged (mean annual shown here) wind field can be seen in  
375 northward winds (Figure 8h) and imply a dynamical contribution to the LAE anomaly patterns

376 via warm air advection. Spatial patterns in these dynamical linkages can help explain some of the  
377 regional anomalies seen in the LAE. For example, we find reduced winds in the North Atlantic  
378 leading to reduced heat loss out of that region. This hints at a tropical teleconnection to the  
379 westerlies (e.g. Hou, 1998), propagating the impact of low latitude geography to the mid  
380 latitudes of the opposite hemisphere, in this case with an amplifying impact on sea ice and  
381 regional warming in the North Atlantic. We observe a positive relationship between the LAE and  
382 500-hPa geopotential height (Figure 8i), whereby a positive “Z500 effect” indicates that the  
383 geopotential heights are regionally higher (implying warm temperatures across the region) when  
384 compared to a symmetric Earth, and vice-versa. Interhemispheric teleconnections like these have  
385 been studied extensively with respect to present day continental geography (Chiang and  
386 Friedman, 2012; Harnack and Harnack, 1985; Hou, 1998; Ji et al., 2014). However, far field  
387 effects such as those arising from interactions between the Hadley circulation and planetary  
388 waves (among other dynamical processes) are not adequately resolved at the relatively coarse  
389 spatial resolution used in these initial simulations, with monthly meteorological output. A more  
390 complete dynamical analysis of the LAE is the subject of ongoing work and a future manuscript.

## 391 **9. Conclusions**

392 The unbalanced fraction of land in the Northern versus Southern Hemisphere has remained  
393 almost unchanged for tens of millions of years. However, the significance of this continental  
394 asymmetry on Earth’s climate response to forcing has not been previously quantified with a  
395 physically based climate models. We find that continental geography of the opposite hemisphere  
396 has a control on the climate system’s response to insolation forcing, and this may help explain  
397 the non-linear response of the Earth’s climate to insolation forcing.

398 According to classical Milankovitch theory, the growth of polar ice sheets at the onset of  
399 glaciation requires cooler summers in the high latitudes, in order for snow to persist throughout  
400 the year. During warm summers at the high latitudes, the winter snowpack melts, inhibiting  
401 glaciation or leading to deglaciation if ice sheets already exist. Thus, the intensity of summer  
402 insolation at high latitudes, especially the Northern polar latitudes, has been considered the key  
403 driver of the glacial-interglacial cycles and other long-term climatic variations. At precessional  
404 periods, at which the high latitude summer insolation intensity primarily varies (Huybers, 2006;  
405 Raymo et al., 2006, etc.), the land asymmetry effect plays an important role by amplifying (and  
406 weakening at certain times) the effect of summer insolation intensity.

407 In all the orbital configurations simulated here, we find that the geography of the Southern  
408 Hemisphere weakens the temperature response of the high Northern Hemisphere latitudes to  
409 orbital forcing. Consequently, this leads to a larger latitudinal gradient in summer temperatures  
410 in the Northern Hemisphere compared to that of a symmetric Earth. In particular, the  
411 amplification (or weakening) of the response to insolation changes at precessional and obliquity  
412 periods might explain some of the important features of late Pliocene-early Pleistocene climate  
413 variability, when obliquity-paced cyclicity dominated precession in global benthic  $\delta^{18}\text{O}$  records.  
414 In Figure 7, we have demonstrated that the interhemispheric effect causes a suppression of the  
415 effects of precessional cycle on the Earth's surface. In other words, the real Earth has a smaller  
416 response to a precession cycle as compared to the hypothetical symmetric Earth. We have also  
417 showed that the interhemispheric effect causes an amplification of the effects of obliquity cycle  
418 on the Earth's surface. In other words, the real Earth has a larger response to the obliquity cycle  
419 in the ocean dominated Southern Hemisphere, as compared to the hypothetical symmetric Earth.  
420 Consequently, the interhemispheric effect of continental geography contributes to the muting of

421 precessional signal and amplification of obliquity signal recorded in paleoclimate proxies such as  
422 benthic  $\delta^{18}\text{O}$  isotope records.

423 There are various ways in which the Earth's continental asymmetry affects climate. Here, we  
424 have shown how these interhemispheric effects influence the Earth's climate response to orbital  
425 forcing via the radiative and atmospheric dynamical processes represented in a slab-ocean GCM.  
426 While computationally challenging, future work should include complimentary simulations with  
427 AOGCMs, to explore the potential modifying role of ocean dynamics on the amplifying and  
428 weakening interhemispheric responses to orbital forcing demonstrated here.

#### 429 **10. Data Availability**

430 The GENESIS GCM model output that was generated for this study is archived under  
431 <http://dx.doi.org/10.17632/kt8v7ths6p.1> (Roychowdhury et al, 2019).

432

433 **Table 1. Experimental Setup of Model Boundary Conditions and Forcings**

Run ID	LSX Configuration	Eccentricity	Obliquity	Precession <sup>a</sup>	GHGs
CONTROL <sub>NHSP</sub>	Modern	0.034	23.2735	270° (NHSP)	Preindustrial
CONTROL <sub>SHSP</sub>	Modern	0.034	23.2735	90° (SHSP)	Preindustrial
CONTROL <sub>EP1</sub>	Modern	0.034	23.2735	0° (EP1)	Preindustrial
CONTROL <sub>EP2</sub>	Modern	0.034	23.2735	180° (EP2)	Preindustrial
CONTROL <sub>HIGH</sub>	Modern	0.034	24.5044	180°	Preindustrial
CONTROL <sub>LOW</sub>	Modern	0.034	22.0425	180°	Preindustrial
NORTH-SYMM <sub>NHSP</sub>	North-symmetric	0.034	23.2735	270° (NHSP)	Preindustrial
NORTH-SYMM <sub>SHSP</sub>	North-symmetric	0.034	23.2735	90° (SHSP)	Preindustrial
NORTH-SYMM <sub>EP1</sub>	North-symmetric	0.034	23.2735	0° (EP1)	Preindustrial
NORTH-SYMM <sub>EP2</sub>	North-symmetric	0.034	23.2735	180° (EP2)	Preindustrial
NORTH-SYMM <sub>HIGH</sub>	North-symmetric	0.034	24.5044	180°	Preindustrial
NORTH-SYMM <sub>LOW</sub>	North-symmetric	0.034	22.0425	180°	Preindustrial
SOUTH-SYMM <sub>NHSP</sub>	South-symmetric	0.034	23.2735	270° (NHSP)	Preindustrial
SOUTH-SYMM <sub>SHSP</sub>	South-symmetric	0.034	23.2735	90° (SHSP)	Preindustrial
SOUTH-SYMM <sub>EP1</sub>	South-symmetric	0.034	23.2735	0° (EP1)	Preindustrial
SOUTH-SYMM <sub>EP2</sub>	South-symmetric	0.034	23.2735	180° (EP2)	Preindustrial
SOUTH-SYMM <sub>HIGH</sub>	South-symmetric	0.034	24.5044	180°	Preindustrial
SOUTH-SYMM <sub>LOW</sub>	South-symmetric	0.034	22.0425	180°	Preindustrial

434 **NHSP:** Northern Hemisphere Summer Solstice at Perihelion

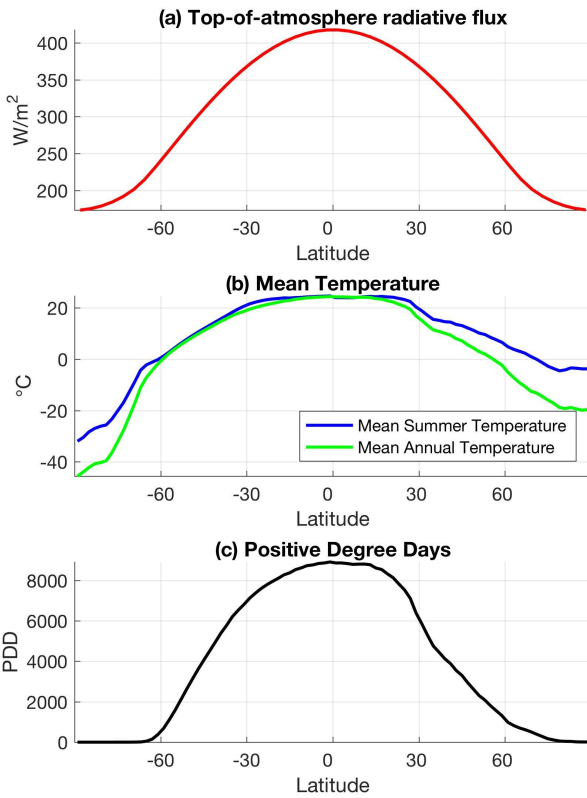
435 **SHSP:** Southern Hemisphere Summer Solstice at Perihelion

436 **EP1:** Northern Hemisphere Vernal Equinox at Perihelion

437 **EP2:** Northern Hemisphere Autumnal Equinox at Perihelion

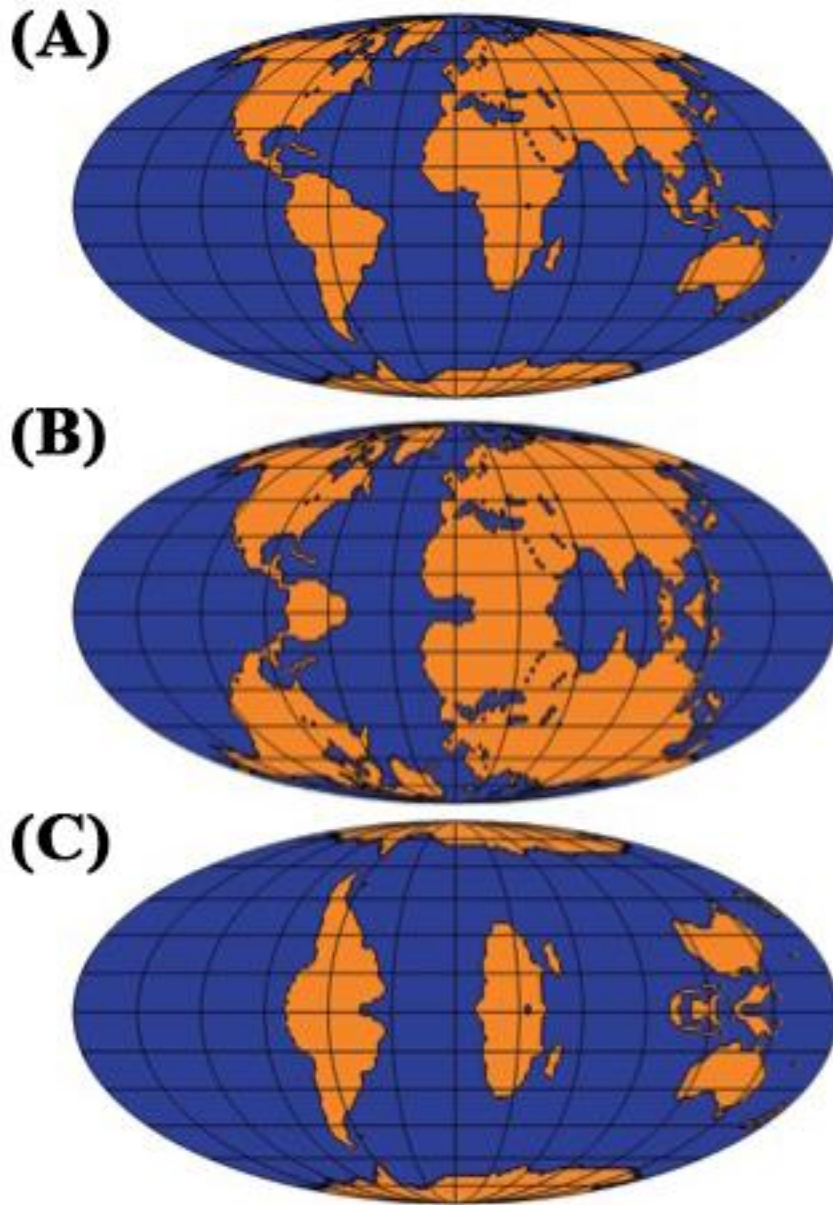
438 <sup>a</sup> Orbital precession in the GCM is defined here as the prograde angle from perihelion to the

439 Northern Hemispheric vernal equinox.



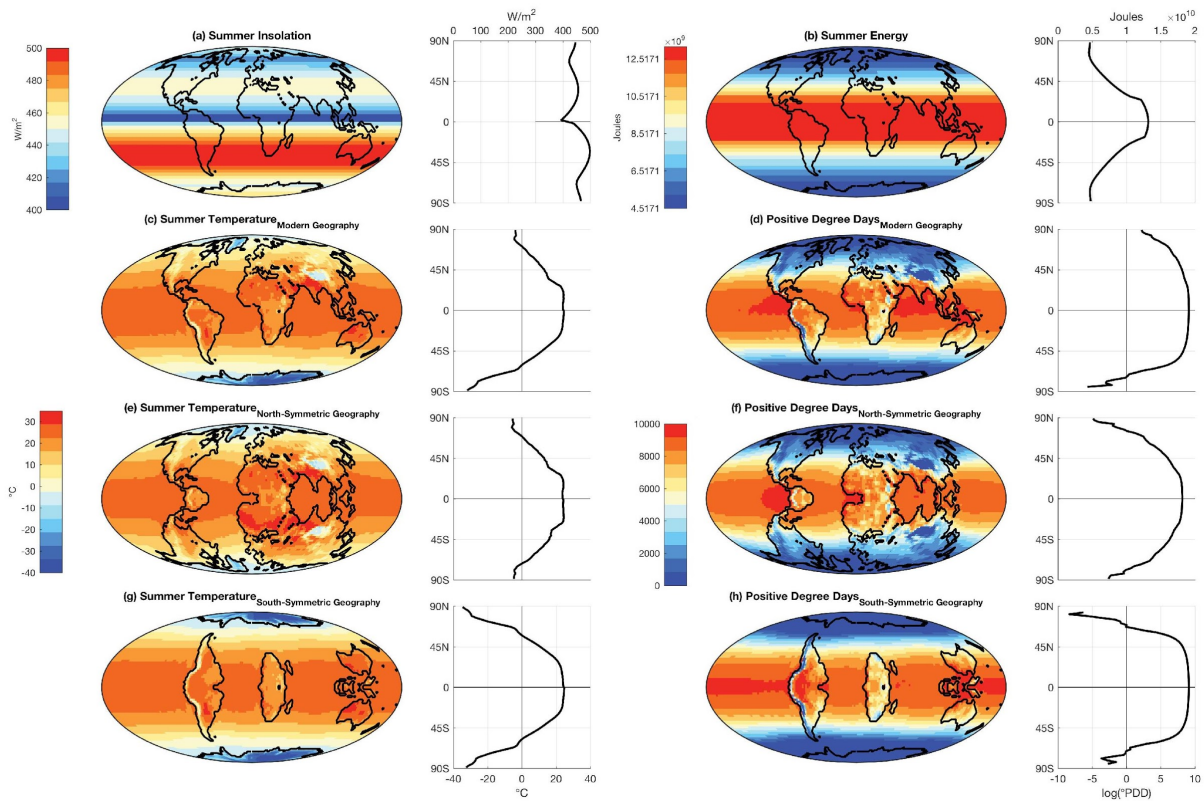
440

441 **Figure 1:** (a) Top-of-atmosphere net incoming radiation (annual mean). (b) Mean Summer  
 442 Temperatures (blue) and Mean Annual Temperatures (green), computed from GCM simulations  
 443 with a modern orbit (c) Positive Degree Days (PDD) calculated from GCM simulations with a  
 444 modern orbit.



445

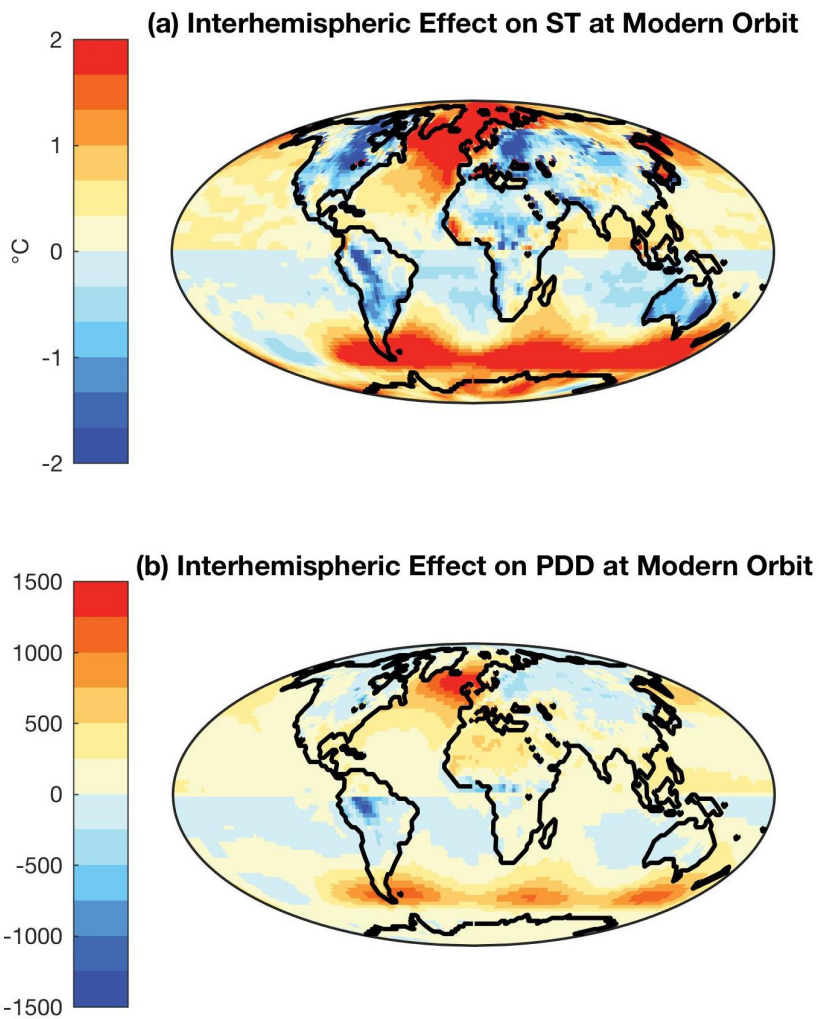
446 **Figure 2:** (A) Modern continental geography (B) NORTH-SYMM geography and (C) SOUTH-  
447 SYMM geography



448

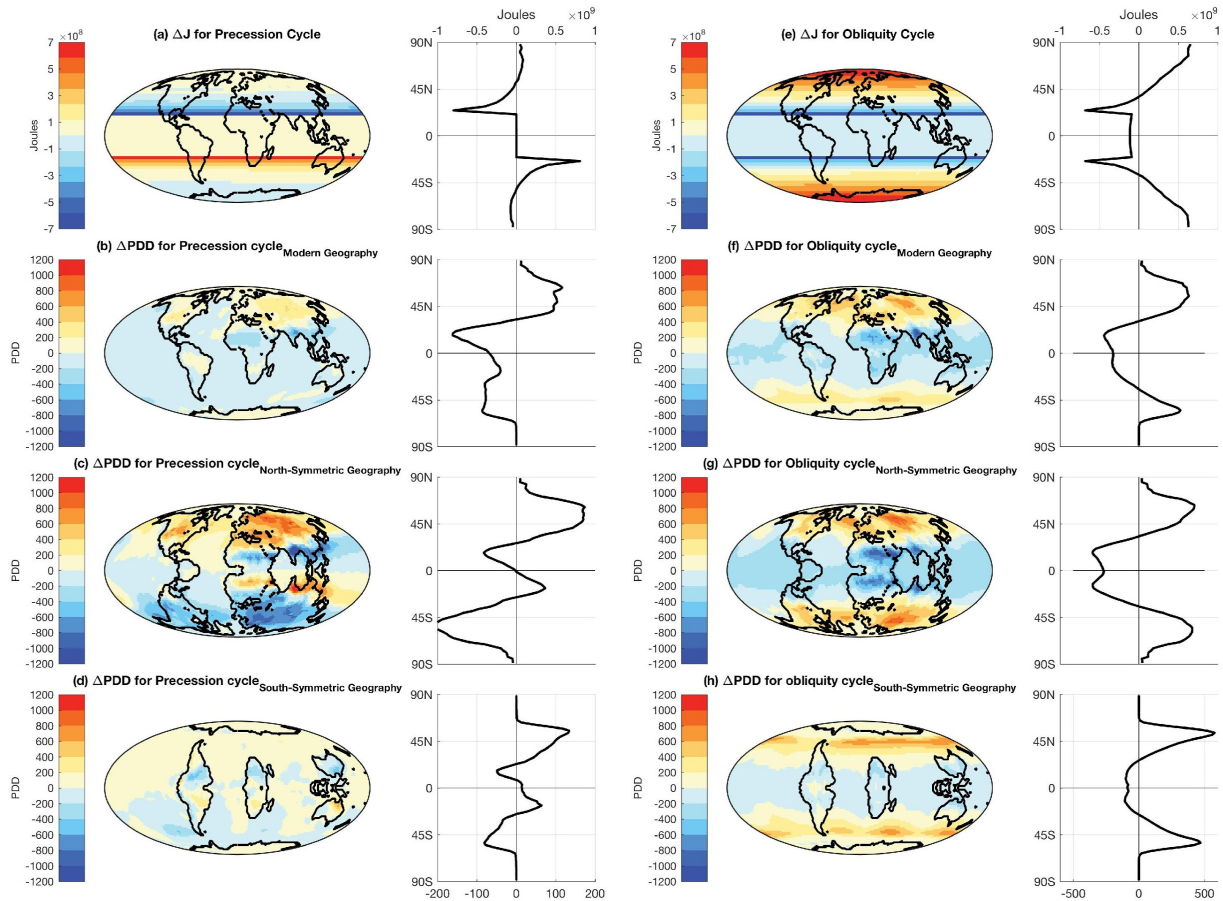
449 **Figure 3:** (a-d) Demonstration of Earth's asymmetric climate response to symmetric climate  
 450 forcing. Simulations are forced with modern orbit: (a) Summer insolation; (b) summer energy (as  
 451 defined in Huybers, 2006); (c) Summer Temperature; and (d) PDD. (e-h) Demonstration of  
 452 Earth's symmetric climate response to climate forcing when idealized symmetric Earth  
 453 geographies are used. Simulations are forced by modern day orbit: (e) and (f) Summer  
 454 Temperature and PDD for NORTH-SYMM simulation, (g) and (h) Summer Temperature and  
 455 PDD for SOUTH-SYMM simulation. The zonal averages are plotted on the right of each Figure.  
 456 Zonal averages of PDD are plotted on a log scale.





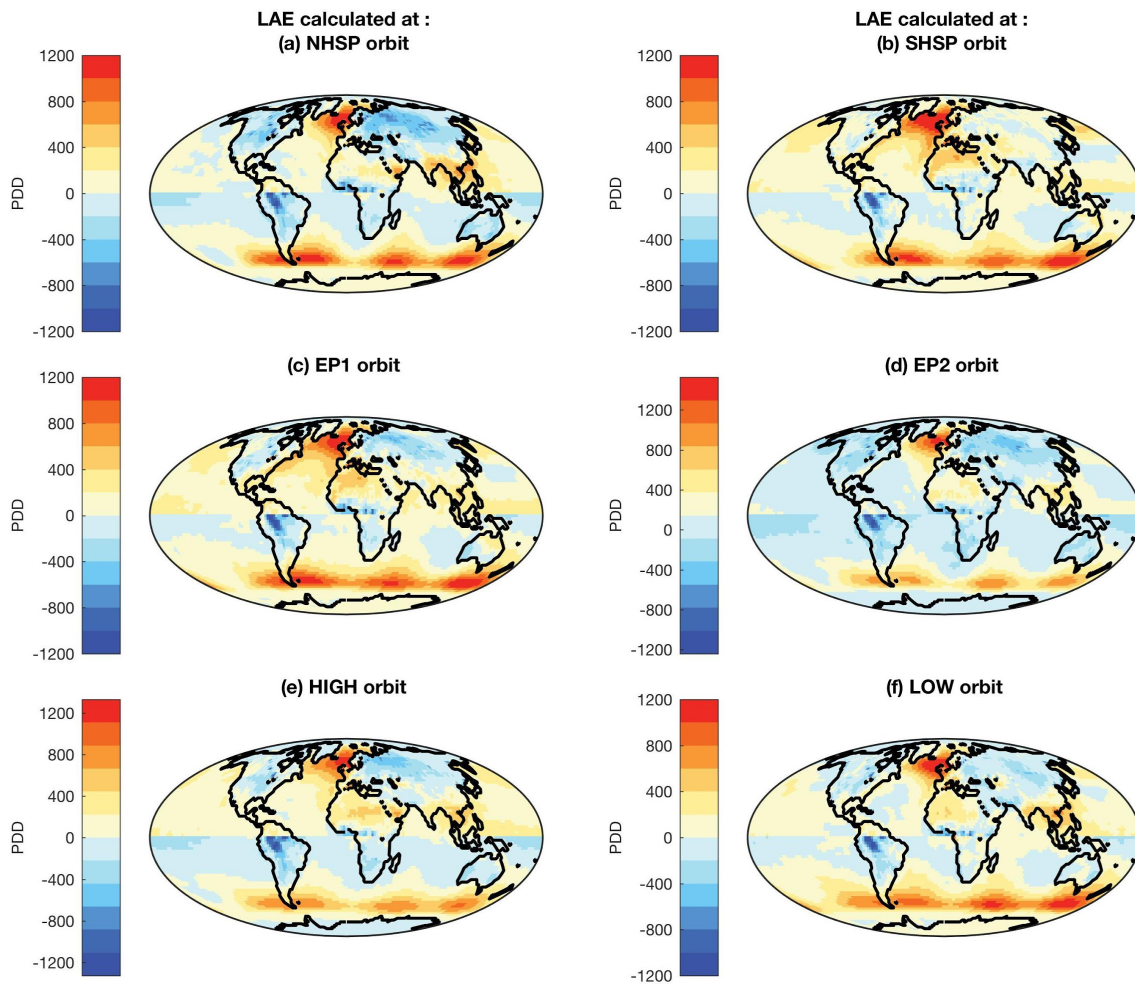
457

458 **Figure 4:** Interhemispheric effect of continental geography (LAE) on: (a) Mean Summer  
459 Temperature (ST) and (b) Positive Degree Days (PDD).



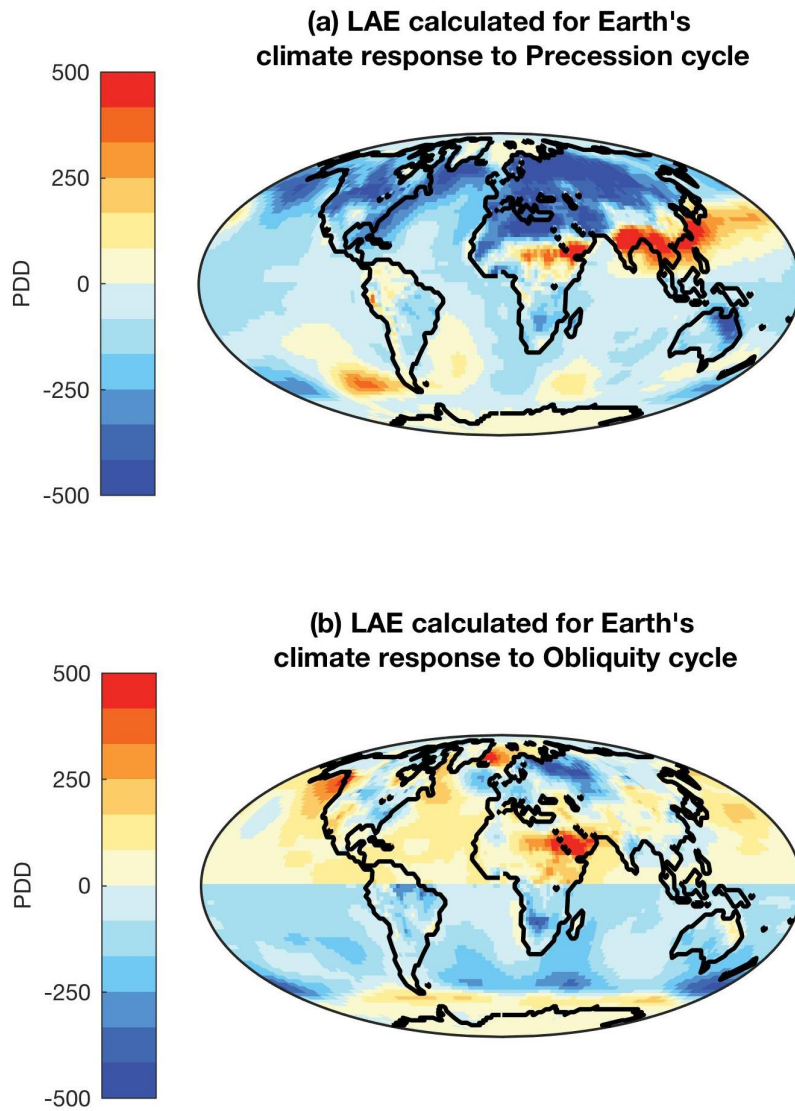
460

461 **Figure 5:** Summer Energy (J) change for a transition from SHSP to NHSP orbit (a); and the  
 462 corresponding change in Positive Degree Days (PDD) in CONTROL (b); NORTH-SYMM (c)  
 463 and SOUTH-SYMM (d) simulations. Summer Energy (J) change for a transition from LOW to  
 464 HIGH orbit (e); and the corresponding change in PDD in CONTROL (f); NORTH-SYMM (g)  
 465 and SOUTH-SYMM (h) simulations.



466

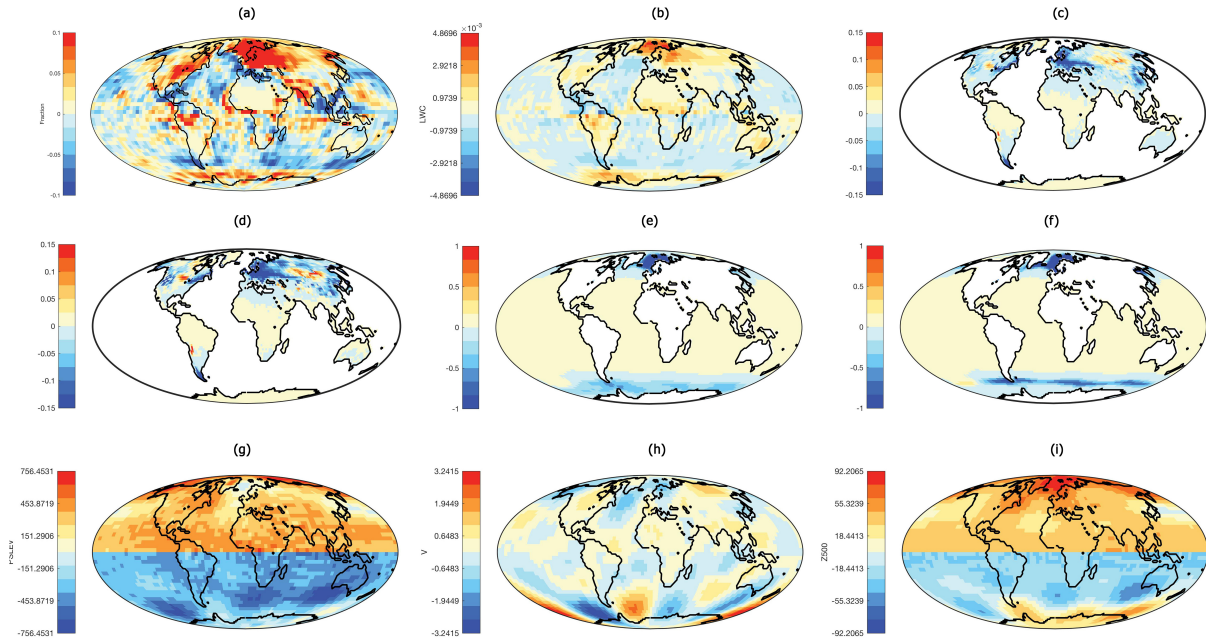
467 **Figure 6:** Interhemispheric effect of continental geography (LAE) on the climate response  
 468 (PDD) at: (a) Northern Hemisphere summer at perihelion; (b) Southern Hemisphere summer at  
 469 perihelion; (C) Northern Hemisphere vernal equinox at perihelion; (d) Northern Hemisphere  
 470 autumnal equinox at perihelion; (e) High obliquity orbit; and (f) Low obliquity orbit.



471

472 **Figure 7:** Interhemispheric effect of continental geography on the climate response to: (a)

473 precession cycle (SHSP to NHSP); and (b) obliquity cycle (Low to High).



474

475 **Figure 8:** The effect of interhemispheric continental distribution on: (a) Mean annual cloud  
 476 cover fraction (b) Liquid water content from all cloud types (kg/kg) (c) Fractional snow cover  
 477 (annual mean) (d) Fractional snow cover (averaged over spring months) (e) Fractional sea ice  
 478 cover (annual mean) (f) Fractional sea ice cover (averaged over spring months) (g) Sea level  
 479 pressure (Pa, annual mean) (h) Northward wind (m/s, annual mean) (i) 500 hPa geopotential  
 480 height (m, annual mean).

481

482 Alder, J. R., Hostetler, S. W., Pollard, D. and Schmittner, A.: Evaluation of a present-day climate  
483 simulation with a new coupled atmosphere-ocean model GENMOM, *Geosci. Model Dev.*, 4(1),  
484 69–83, doi:10.5194/gmd-4-69-2011, 2011.

485 Barron, E. J., Thompson, S. L. and Hay, W. W.: Continental distribution as a forcing factor for  
486 global-scale temperature, *Nature*, 310(5978), 574–575, doi:10.1038/310574a0, 1984.

487 Berger, A. and Loutre, M. F.: Insolation values for the climate of the last 10 million years, *Quat.*  
488 *Sci. Rev.*, 10(4), 297–317, doi:10.1016/0277-3791(91)90033-Q, 1991.

489 Bonan, G. B., Pollard, D. and Thompson, S. L.: Effects of boreal forest vegetation on global  
490 climate, *Nature*, 359(6397), 716–718, doi:10.1038/359716a0, 1992.

491 Charles Lyell: *Principles of Geology*, John Murray: Albemarle Street, London. [online]  
492 Available from: <https://www.bl.uk/collection-items/charles-lyells-principles-of-geology#>  
493 (Accessed 31 January 2018), 1832.

494 Chiang, J. C. H. and Friedman, A. R.: Extratropical Cooling, Interhemispheric Thermal  
495 Gradients, and Tropical Climate Change, *Annu. Rev. Earth Planet. Sci.*, 40(1), 383–412,  
496 doi:10.1146/annurev-earth-042711-105545, 2012.

497 Croll, J.: On ocean-currents, part I: ocean-currents in relation to the distribution of heat over the  
498 globe., *Philos. Mag. J. Sci.*, 39(259), 81–106, 1870.

499 Cuming, M. J. and Hawkins, B. A.: TERDAT: The FNOC system for terrain data extraction and  
500 processing. Tech. Rep. M11 Project M254, 2d ed. [Available from U.S. Navy Fleet Numerical  
501 Oceanography Center, Code 42, Monterey, CA 93943, 1981.

502 Deconto, R. M., Pollard, D., Wilson, P. A., Pälike, H., Lear, C. H. and Pagani, M.: Thresholds  
503 for Cenozoic bipolar glaciation., *Nature*, 455(7213), 652–6, doi:10.1038/nature07337, 2008.

504 Flato, G. M. and Boer, G. J.: Warming asymmetry in climate change simulations, *Geophys. Res.*  
505 *Lett.*, 28(1), 195–198, doi:10.1029/2000GL012121, 2001.

506 Harnack, R. P. and Harnack, J.: Intra- and inter-hemispheric teleconnections using seasonal  
507 southern hemisphere sea level pressure, *J. Climatol.*, 5(3), 283–296,  
508 doi:10.1002/joc.3370050305, 1985.

509 Hay, W. W., Barron, E. J. and Thompson, S. L.: Results of global atmospheric circulation  
510 experiments on an Earth with a meridional pole-to- pole continent, *J. Geol. Soc. London.*,  
511 147(2), 385–392, doi:10.1144/gsjgs.147.2.0385, 1990.

512 Hou, A. Y.: Hadley Circulation as a Modulator of the Extratropical Climate, *J. Atmos. Sci.*,  
513 55(14), 2437–2457, doi:10.1175/1520-0469(1998)055<2437:HCAAMO>2.0.CO;2, 1998.

514 Huybers, P.: Early Pleistocene glacial cycles and the integrated summer insolation forcing.,  
515 *Science*, 313(5786), 508–11, doi:10.1126/science.1125249, 2006.

516 Ji, X., Neelin, J. D., Lee, S.-K., Mechoso, C. R., Ji, X., Neelin, J. D., Lee, S.-K. and Mechoso, C.  
517 R.: Interhemispheric Teleconnections from Tropical Heat Sources in Intermediate and Simple  
518 Models, *J. Clim.*, 27(2), 684–697, doi:10.1175/JCLI-D-13-00017.1, 2014.

519 Kang, S. M., Seager, R., Frierson, D. M. W. and Liu, X.: Croll revisited: Why is the northern  
520 hemisphere warmer than the southern hemisphere?, *Clim. Dyn.*, doi:10.1007/s00382-014-2147-z,  
521 2014.

522 Kiehl, J. T., Hack, J. J., Bonan, G. B., Boville, B. a., Williamson, D. L. and Rasch, P. J.: The  
523 National Center for Atmospheric Research Community Climate Model: CCM3\*, *J. Clim.*, 11(6),  
524 1131–1149, doi:10.1175/1520-0442(1998)011<1131:TNCFAR>2.0.CO;2, 1998.

525 Kineman, J.: FNOC/NCAR global elevation, terrain, and surface characteristics, Digital Dataset.,  
526 1985.

527 Koenig, S. J., DeConto, R. M. and Pollard, D.: Pliocene Model Intercomparison Project  
528 Experiment 1: implementation strategy and mid-Pliocene global climatology using GENESIS  
529 v3.0 GCM, *Geosci. Model Dev.*, 5(1), 73–85, doi:10.5194/gmd-5-73-2012, 2012.

530 Loutre, M.-F., Paillard, D., Vimeux, F. and Cortijo, E.: Does mean annual insolation have the  
531 potential to change the climate?, *Earth Planet. Sci. Lett.*, 221(1–4), 1–14, doi:10.1016/S0012-  
532 821X(04)00108-6, 2004.

533 Manabe, S., Wetherald, R. T., Manabe, S. and Wetherald, R. T.: Thermal Equilibrium of the  
534 Atmosphere with a Given Distribution of Relative Humidity, *J. Atmos. Sci.*, 24(3), 241–259,  
535 doi:10.1175/1520-0469(1967)024<0241:TEOTAW>2.0.CO;2, 1967.

536 Meinshausen, M., Smith, S. J., Calvin, K., Daniel, J. S., Kainuma, M. L. T., Lamarque, J.-F.,  
537 Matsumoto, K., Montzka, S. A., Raper, S. C. B., Riahi, K., Thomson, A., Velders, G. J. M. and  
538 van Vuuren, D. P. P.: The RCP greenhouse gas concentrations and their extensions from 1765 to  
539 2300, *Clim. Change*, 109(1–2), 213–241, doi:10.1007/s10584-011-0156-z, 2011.

540 Meleshko, V. P. and Wetherald, R. T.: The effect of a geographical cloud distribution on climate:  
541 A numerical experiment with an atmospheric general circulation model, *J. Geophys. Res.*,



542 86(C12), 11995, doi:10.1029/JC086iC12p11995, 1981.

543 Philander, S. G. H., Gu, D., Lambert, G., Li, T., Halpern, D., Lau, N.-C. and Pacanowski, R. C.:  
544 Why the ITCZ Is Mostly North of the Equator, *J. Clim.*, 9(12), 2958–2972, doi:10.1175/1520-  
545 0442(1996)009<2958:WTIIMN>2.0.CO;2, 1996.

546 Raymo, M. E., Lisiecki, L. E. and Nisancioglu, K. H.: Plio-Pleistocene Ice Volume, Antarctic  
547 Climate, and the Global d18O Record, , 313(July), 492–495, 2006.

548 Schneider, S. H.: Cloudiness as a Global Climatic Feedback Mechanism: The Effects on the  
549 Radiation Balance and Surface Temperature of Variations in Cloudiness, *J. Atmos. Sci.*, 29(8),  
550 1413–1422, doi:10.1175/1520-0469(1972)029<1413:CAAGCF>2.0.CO;2, 1972.

551 Short, D. A., Mengel, J. G., Crowley, T. J., Hyde, W. T. and North, G. R.: Filtering of  
552 Milankovitch Cycles by Earth’s Geography, *Quat. Res.*, 35(02), 157–173, doi:10.1016/0033-  
553 5894(91)90064-C, 1991.

554 Stone, P. H.: Constraints on dynamical transports of energy on a spherical planet, *Dyn. Atmos.*  
555 *Ocean.*, 2(2), 123–139, doi:10.1016/0377-0265(78)90006-4, 1978.

556 Stouffer, R. J., Manabe, S. and Bryan, K.: Interhemispheric asymmetry in climate response to a  
557 gradual increase of atmospheric CO<sub>2</sub>, *Nature*, 342(6250), 660–662, doi:10.1038/342660a0,  
558 1989.

559 Thompson, S. L. and Pollard, D.: Greenland and Antarctic Mass Balances for Present and  
560 Doubled Atmospheric CO<sub>2</sub> from the GENESIS Version-2 Global Climate Model, *J. Clim.*,  
561 10(5), 871–900, doi:10.1175/1520-0442(1997)010<0871:GAAMBF>2.0.CO;2, 1997.

562 Trenberth, K. E., Fasullo, J. T., Kiehl, J., Trenberth, K. E., Fasullo, J. T. and Kiehl, J.: Earth's  
563 Global Energy Budget, *Bull. Am. Meteorol. Soc.*, 90(3), 311–323,  
564 doi:10.1175/2008BAMS2634.1, 2009.

565 Wetherald, R. T., Manabe, S., Wetherald, R. T. and Manabe, S.: Cloud Cover and Climate  
566 Sensitivity, *J. Atmos. Sci.*, 37(7), 1485–1510, doi:10.1175/1520-  
567 0469(1980)037<1485:CCACS>2.0.CO;2, 1980.

568